Unique Similarity of the Asymmetric Trehalose Solid-State Hydration and the Diluted Aqueous-Solution Hydration

ARTICLE *in* THE JOURNAL OF PHYSICAL CHEMISTRY B · SEPTEMBER 2000

Impact Factor: 3.3 · DOI: 10.1021/jp000943i

2 AUTHORS:

Søren Balling Engelsen
University of Copenhagen
254 PUBLICATIONS **5,873** CITATIONS
SEE PROFILE

Serge Perez
French National Centre for Scientific Researc…
296 PUBLICATIONS **8,315** CITATIONS
SEE PROFILE

Unique Similarity of the Asymmetric Trehalose Solid-State Hydration and the Diluted Aqueous-Solution Hydration

Søren B. Engelsen[†] and Serge Pérez*[,‡]

Department of Dairy and Food Science, Food Technology, The Royal Veterinary and Agricultural University, Rolighedsvej 30, DK-1958 Frederiksberg C, Denmark, and Centre de Recherches sur les Macromolécules Végétales, CNRS, BP 53X, 38041 Grenoble cédex, France. Affiliated with the Université Joseph Fourier at Grenoble

Received: March 13, 2000; In Final Form: July 6, 2000

The structural and dynamical features of the hydration of the disaccharide α,α-trehalose have been derived from a 2.5 ns molecular dynamics with an explicit representation of the water molecules. The study aims at establishing a comprehensive understanding of the hydration pattern of trehalose and comparing such features with those displayed by sucrose. The homonuclear and heteronuclear coupling constants, the overall molecular tumbling time, and self-diffusion coefficient of the trehalose in aqueous solutions were established from the molecular dynamics simulations and compare well with experimental data. While the calculated translational diffusion of trehalose is very similar to that of sucrose, the calculated rotational diffusion is much slower. The presence of water in the simulation induces significant changes in the mean potential acting on trehalose. It generates an asymmetric mean structure between the two glucose rings, in the otherwise symmetrical trehalose. The analysis of the hydration characteristics provides an average molecular hydration number of 7.8 water molecules in the first hydration shell which is close to that derived experimentally from viscosity and apparent molar volume. Average and maximum residence times for water molecules around the trehalose solute were also characterized. The analysis revealed that the water molecules around the O-2 hydroxyl groups were the most resident and that the water molecules around the acetalic oxygens in the "central cavity" of trehalose were particular mobile. 2D radial pair distributions were calculated to analyze the solute surroundings for localized water densities, e.g., bridging water molecules between the two pyranose rings. This analysis revealed no strong first hydration shell interactions, as found in the case of sucrose, but revealed that the water molecules of the dihydrate solid-state structure are largely capable of satisfying the "hydration requirements" of the solute.

Introduction

Mushroom sugar or α,α-trehalose is the only naturally occurring out of three isomeric trehalose forms, and has a hydration characteristic, which displays extremely interesting features. It has been found to be the key substance produced by many cryptobionts in both the plant and animal kingdoms including desert insects, brine shrimp embryo, baker's yeast, spores of certain fungi, and a few varieties of plant seeds. Survival of anhydrobiosis and cryptobiosis by many of these organisms was in the early 1980s found to be correlated with the presence of trehalose by Crowe and co-workers.[1,2] Since then, with research mainly driven by the potential interests in medical protein stability and food preservation, trehalose has been subjected to a large number of physical, chemical, and biological functional studies. The major results obtained are the following: (i) the ability of trehalose to protect and reversibly restitute proteins and bio-membranes from dehydration including the freeze-drying cycles;[3,4] (ii) that the trehalose−water system possesses a significantly higher glass-transition temperature than other related disaccharides, also called the trehalose anomaly;[5] (iii) the ability to retain and preserve volatile flavors and aromas in trehalose-dried foodstuff;[6] (iv) and most recently the ability of trehalose to preserve mammalian cells during freezing and drying.[7]

While the detailed X-ray crystal structure of α,α-trehalose dihydrate was reported as early as in 1972[8,9] and the low-temperature anhydrous structure in 1985,[10] they provided no clues to explain the structural mechanism(s) responsible for the unique functional properties of trehalose. To elucidate these mechanisms trehalose has been subjected to a number of experimental and theoretical studies including solid-state infrared[11,12] and NMR[13,14] studies of dehydrated lipid bilayers in the presence of trehalose. In solution state, trehalose has been studied by NMR[15] and optical rotation.[16] However, only very recently has trehalose been studied by NMR using [1-^{13}C]-labeled trehalose to avoid the problems for characterization of the solution conformation caused by its C_2 molecular symmetry.[17]

Trehalose has also been subjected to molecular modeling studies as a complementary method to decipher some of its the structural features. In a vacuum, the detailed structure of trehalose has been investigated by Tvaroska and Vaclavik[18] using the MM2CARB force field; it has been followed up by a study by Dowd et al.[19] using the MM3 force field. Trehalose interactions with lipids have also been investigated using molecular modeling by Rudolph et al.[20] However, with the aim

* Author to whom correspondence should be addressed. Tel: 33-476-03-76-30. Fax: 33-476-03-76-29. E-mail: perez@cermav.cnrs.fr.
[†] The Royal Veterinary and Agricultural University.
[‡] Centre de Recherches sur les Macromolécules Végétales, CNRS.

10.1021/jp000943i CCC: $19.00
Published on Web 09/08/2000

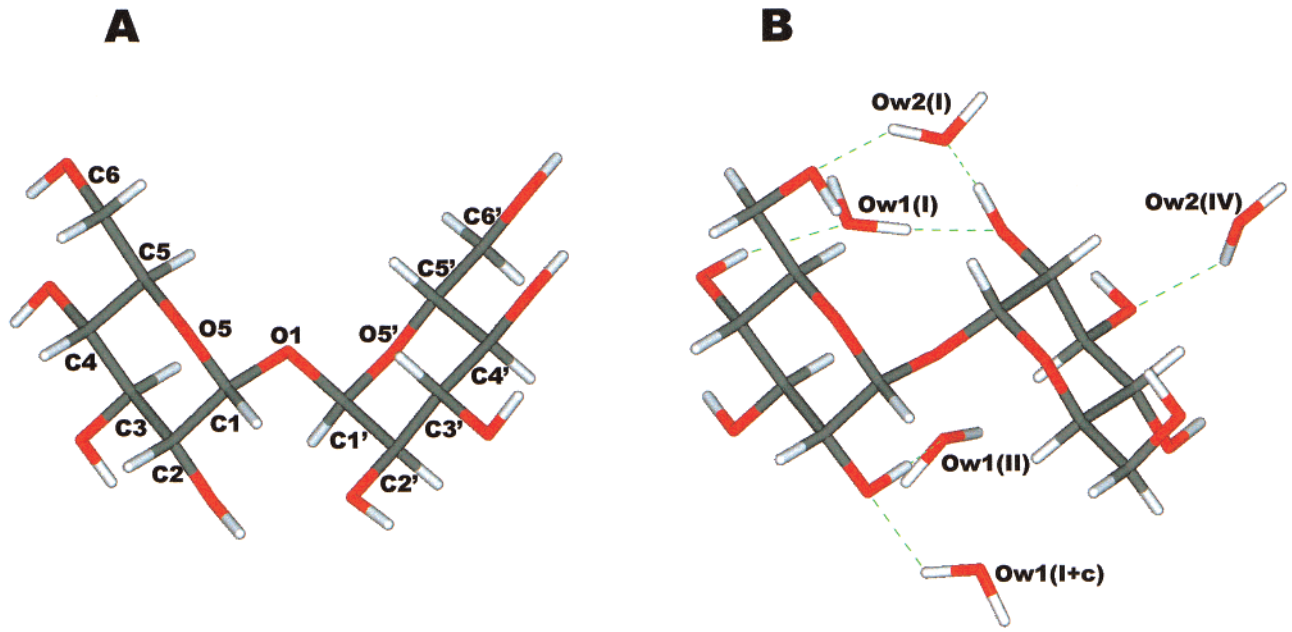

Figure 1. Molecular structure of α,α-trehalose including atomic labels. (A) The symmetric global minimum, and (B) the hydrated conformation of trehalose molecule surrounded by the five close neighbor water molecules as found in the crystalline structure.[8]

of understanding the underlying mechanisms behind the anomaly and the cryo-protective properties of trehalose it is considered of fundamental importance to characterize the structural features of hydration. Two molecular dynamics studies considering the interaction of trehalose with water have been reported in the literature. Donnamaria et al.[21] studied trehalose in an aqueous solution from a 100 ps molecular dynamics simulation using the GROMOS force field[22] and 270 SPC/E waters,[23] concluding that the water structure was not significantly perturbed by the presence of trehalose. Liu et al.[24] later performed a 130 + 300 ps simulation of trehalose, using the CHARMM force field,[25] solvated in 488 TIP3P waters[26] and concluded that trehalose as other sugars perturbs the water structure, but that trehalose does not appear to be unique in its solvation properties.

The present study aims at complementing the latter MD study by following the trehalose dynamics and hydration for a total of 2.5 ns divided on three micro-canonical trajectories and by comparing the results with NMR observables. Furthermore, the results are compared with the crystalline hydration of the trehalose dihydrate and with the hydration of another nonreducing disaccharide, sucrose.[27] Sucrose shares with trehalose a number of properties including nonreducing stability, the ability to protect macromolecules against dehydration, and sweet taste induction.[28] In this study, the trehalose−water interactions as viewed from the MD trajectories are analyzed by the calculation of NMR parameters such as coupling constants, macroscopic observables such as translation and rotational diffusion, hydration numbers, and hydrodynamic radius of gyration. Finally, the hydration pattern is examined by calculating pair distribution functions, residence times of water molecules, perturbation of the structure of water induced by the solute, and searching for highly localized water molecules around the solute by 2D pair distributions.[29]

Methods

Nomenclature. α,α-trehalose (α-D-Glc*p*-(1−1)-α-D-Glc*p*) is one of three isomeric forms (αα, α*β*, and *ββ*) of nonreducing disaccharides collectively known as the trehaloses. In the (C_2) symmetric α,α-trehalose two α-d-glycosyl units are linked by a glycosidic linkage between their two anomeric carbon atoms, abbreviated to as C-1 g and C-1 g′, exhibiting the so-called double anomeric effect. A model of α,α-trehalose, including labeling of the oxygen atoms is shown in Figure 1. Conformational flexibility around the glycosidic linkage bonds is described by the two torsional angles: Φ = O-5g−C-1g−O-1g−C-1g′ and Φ′= C-1g−O-1g−C-1g′−O-5g′, and the conformations of the two hydroxymethyl groups are described by the torsional angles: ω_g = O-5g−C-5g−C-6g−O-6g and $\omega_{g'}$ = O-5g′−C-5g′−C-6g′−O-6g′. The three staggered orientations of the primary hydroxyl groups are also referred to as either gauche−gauche (GG), gauche−trans (GT), or trans−gauche (TG), depending on whether the values of the above torsion angles are closest to −60°, 60°, or 180°, respectively. The sign of the torsion angles is defined in agreement with the IUPAC Commission of Biochemical Nomenclature.[30]

Molecular Dynamics. The solution behavior of trehalose was investigated by calculating a total ensemble of 2.5 (1 + 0.75 + 0.75) ns molecular dynamics (MD) trajectories in an explicit water phase from three micro-canonical trajectories (constant *n*, *V*, *T*) where the initial coordinates of the solute were taken as the crystalline dihydrate structure[8] and as the symmetric perfectly staggered form which happened to be the global minimum in the applied force field. The molecular dynamics simulations were performed by using the carbohydrate force field[25] implemented in the general molecular mechanics CHARMM program.[31] The water molecules of the solvent were modeled using the TIP3P potential energy function.[26] In the simulation, Newton's equations of motion were integrated for each atom using the two-step velocity Verlet algorithm.[32] All hydrogen atoms were explicitly included in the simulations, although bond lengths involving hydrogen atoms were kept fixed throughout the simulation using the constraint algorithm SHAKE.[33] When these fastest atomic motions are removed, the step size of 1 fs in the integration algorithm is far from the theoretical stability limit ($\Delta t = \omega_{min}/\pi$) and well below the practical stability limit of the Verlet algorithm.[33] The explicit water phase was mimicked in the form of 512 water molecules captured in a cubic box using minimum image boundary

conditions. Interactions between atoms more than 12 Å apart were truncated, and switching functions were used to smoothly turn off long-range interactions between 10 and 11 Å. The coordinates of the crystalline conformation of trehalose were superimposed upon the coordinates of a well-equilibrated (at 300 K) box of pure TIP3P water. This procedure left 485 water molecules in the primary box when deleting those water molecules whose van der Waals radii overlapped with any of the atoms of the solute, resulting in an actual concentration of approximately 4 %(w/w). After this virtual solvation, the system was energy minimized with 50 steepest descent iterations with the original box size in order to relax steric conflicts that might have been created in the generation of the box and in order to relax the solute structure in the new environment. Then the cubic box length was slightly adjusted to give the experimental density of 1.013 g/cm^3. Initial velocity for all atoms was assigned from a Boltzman distribution at 300 K. The system was equilibrated for 50 ps to relax any artificial starting conditions produced by the solvation procedure, with occasional scaling of the atomic velocities when the average temperature deviated from the desired temperature of 300 K by more than an acceptable tolerance of ±3 K. Following the equilibration period, the Verlet integration was continued without any further interference for subsequent 950 ps. Complete phase points were saved every 0.02 ps for subsequent analysis.

Analysis of Solute Structure. The main degree of flexibility of the trehalose molecule, namely, across the glycosidic linkage, is investigated as simple time series of Φ and Φ′ as well as from population maps derived from molecular dynamics. For reference purposes the potential energy surface in (Φ, Φ′)-space of trehalose was computed from 36 individual relaxed potential energy maps in a vacuum using the same force field. The starting conformations of the pyranosyl groups were in all cases taken as $^4C_1$. For all 9 possible combinations of orientations (GG/GT/TG) of ω_g and $\omega_{g'}$, a clockwise (c) and reverse clockwise (r) orientation of the secondary hydroxyl groups on the glucopyranosyl ring were considered. The relaxed maps were computed using rigid rotation followed by harmonic constraint minimization in 10° increments for Φ and Φ′ spanning the whole angular range. Convergence was accepted when the rms gradient was less than 0.001 kcal/mol/Å^2 in the iterative conjugate gradient minimization algorithm. No cutoff of long-range nonbonded interactions was introduced in the energy calculations. For each point on this grid, the optimized coordinates and the corresponding energy were stored for further calculations. This approach resulted in 46656 possible conformations to be evaluated for the construction of a general adiabatic (Φ,Φ′)-map by contouring the lowest energy values.

Population Maps. Normalized population maps are simple two-dimensional histogram representations of the trajectories in (Φ, Φ′)-space. For these calculations the angular range of the dihedral angles are divided into 5° intervals for each histogram bin and divided by the entire number of trajectory frames.

Calculation of Solute Diffusion Processes. The translational diffusion coefficient, *D*, was estimated using the Einstein relation, valid at long times, by calculating the mean square displacement autocorrelation function for the solute center of mass as a function of Δt:[34,35] $D(\Delta t) = \langle|\vec{r}(t+\Delta t) - \vec{r}(t)|^2\rangle/6\Delta t$. After an initial period with free movements followed by a period with backscattering, this function should become equal to the diffusion constant. As the statistical significance deteriorates quickly, this function is only calculated up to $\Delta t = 20$ ps. The overall molecular tumbling time or rotational diffusion for the solute was estimated from the angular evolution of the solute dipole moment, as expressed by the autocorrelation function of the angular displacement of the dipole moment vector as a function of Δt.[35] The rotational diffusion is roughly estimated by the time when the average angular displacement becomes uncorrelated (orthogonal).

Calculation of Coupling Constants. Coupling constants, $^3J_{H,H}$, for vicinal hydrogen atoms of a H−C−C−H segment were calculated using a Karplus type equation with the Haasnoot−Altona parametrization[36] accounting for the *J* dependence on the dihedral angle (Θ) of the H−C−C−H fragment, on the electronegativity of participating atoms, and on the orientation of the α and β substituents. The heteronuclear coupling constant $^3J_{H,C}$ across the glycosidic linkage was calculated by using the equation for the C−O−C−H segment parametrized by Tvaroska et al.[37] Rotamer distributions about primary hydroxyl groups were calculated numerically from the limiting values given by the Haasnoot−Altona equation considering only idealized staggered conformations.

Analysis of Water Structure. Radial atomic pair distribution functions *g(r)* were calculated between selected solute atoms and the water molecules[27] in order to obtain the degree and structure of the solvation of the trehalose. The radial pair distribution function gives the probability of finding a water molecule (oxygen) at a given distance *r* from the solute atom, relative to the probability expected for a random distribution at the same density. The first sphere of nearest neighbors is indicated by a peak in *g(r)* and limited by a minimum in *g(r)* and is referred to as the first hydration shell.

Orientational distribution functions $p(\cos\theta)$ were calculated between selected solute atoms and the O_w-H vectors of the water molecules[27] in order to investigate in more detail the structure of the solvation of trehalose. The orientational distribution functions give the probability of finding a first hydration shell water molecule with at a given O_w-H...O_s angle to the solute oxygen O_s.

Average and maximum residence times, t_{av} *and* t_{max}, of trehalose in aqueous solution were calculated on a frame-by-frame basis, counting all water molecules which did enter the first hydration shell as defined by a solute-oxygen−water-oxygen distance (O_s...O_w) of less than 3.5 Å. We have previously reported residence times of water molecules around sucrose which only took into account one water molecule at a time (frame) and thus were significantly longer.[27] A more thorough description of the residence characteristics, other than average and maximum residence times, would require residence distributions as a function of time.

Total hydration number, ***h***, of the trehalose solute was evaluated by counting all water molecules in a sphere around the oxygen atoms as a function of the radius of the sphere.

*2*D radial pair distributions,[29] $g(r_1, r_2)$, were calculated to analyze the solute surroundings for localized water densities, e.g., bridging water molecules between the two pyranose rings. The 2D radial pair distribution function $g(r_1, r_2)$ gives the probability of finding an atom (e.g., water oxygen) at a distance r_1 and r_2 from two selected solute atoms, relative to the probability expected for a random distribution.

$$g(r_1,r_2) = \frac{N(r_1,r_2)}{\rho_w \times V_{\text{intersect}}(r_1,r_2,\Delta r)} \qquad (1)$$

The calculation of 2D radial pair distributions is analogous to 1D radial pair distribution, except that the histogram is now two-dimensional, referring to two reference points (nuclei)

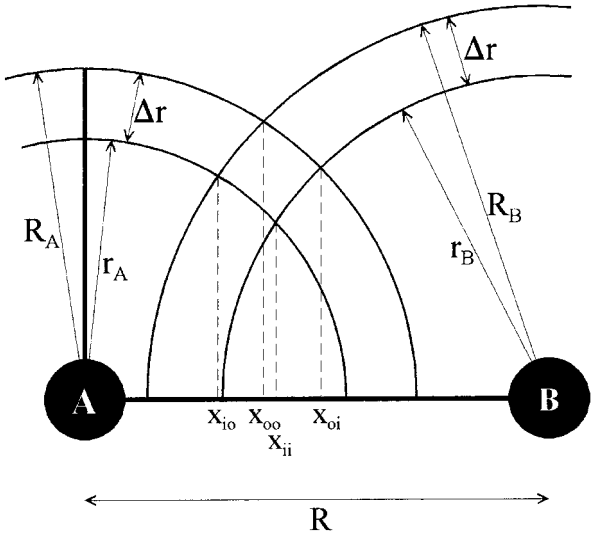

Figure 2. Schematic diagram of hydration shells with indications of relevant parameters for calculating 1D and 2D pair distributions (from ref 29).

instead of one, and the normalization is more complicated. The 2D radial pair distributions have to be normalized using the intersection volume of the two sphere shells, $V_{\text{intersect}}$ in order to be relative to bulk density (equal to 1).

When calculating the intersection volume we consider two atoms, **A** and **B**, connected through their centers by a virtual axis (Figure 2). The center of atom **A** defines the *zero* of the axis, and on this axis the distance between the atoms is R. Two spheres circumscribe atom **A**, the innermost with radius r_A and the outermost with radius R_A. Likewise, two spheres circumscribe atom **B**, with radii r_B and R_B. For both atoms, a spherical cavity (or shell) is defined by the space between the inner and the outer spheres. The thickness of this cavity is equal for **A** and **B**, and is designated $\Delta r = R_A - r_A = R_B - r_B$. The task is to calculate the volume of the intersection of the two spherical cavities. The task of calculating the volume of a sphere section (slice), limited by two planes perpendicular to its radius, is a significant problem in this respect. Let x_1 define the intersection point of the first limiting plane and let x_2 define the intersection point of the second plane on the axis common to both atoms. Initially, an expression is derived for a sphere circumscribing atom **B**, which has its center located at R. For atom **A**, the same solution applies for $R = 0$. Using the nomenclature above, the solution is as described in (2) subject to $(x_1,x_2,r,R \in R | x_1 < x_2 \wedge \{x_1,x_2\} \in [R - r, R + r])$

$$V(x_1,x_2,r,R) = \pi \int_{x_1}^{x_2} y(x,r,R)^2 \, dx$$

$$= \pi \int_{x_1}^{x_2} r_2 - (x - R)^2 \, dx \qquad (2)$$

$$= \frac{\pi}{3}(x_1^3 - x_2^3) + \pi R(x_2^2 - x_1^2) + \pi(x_2 - x_1)(r^2 - R^2)$$

Given V, the problem simplifies to identify x_1 and x_2, since r is either r_A, R_A, r_B, or R_B and R is zero (0) in the case of atom **A**. In the numerical simulation it holds that $\Delta r \ll r_A$. Using this simplification, a number of seven distinct cases can be identified. Not all are equally important, since some are special cases that rarely occur. To simplify the presentation, we define the following scalars:

$$x_{ii} = \frac{1}{2R}(r_a^2 + R^2 - r_b^2)$$

$$x_{io} = \frac{1}{2R}(r_a^2 + R^2 - R_b^2)$$

$$x_{oi} = \frac{1}{2R}(R_a^2 + R^2 - r_b^2)$$

$$x_{oo} = \frac{1}{2R}(R_a^2 + R^2 - R_b^2)$$

Using these definitions, we derive the following seven cases:

Case I $(R - r_B \le -R_A)$

$$V^{I} = 0$$

Case II $(-R_A < R - r_B \le -r_A)$

$$V^{II} = V(-r_A,x_{oi},R_A,0) - V(R - r_B,x_{oi},r_B,R)$$

Case III $(-r_A < R - r_B \le r_A)$

$$V^{III} = V(R - R_B,x_{oo},R_B,R) + V(x_{oo},x_{oi},R_A,0) - V(-r_A,x_{ii},r_A,0) - V(x_{ii},x_{oi},r_B,R)$$

Case IV $(-r_A < R - R_B < R - r_B \le r_A)$

$$V^{IV} = V(x_{io},x_{oo},R_B,R) + V(x_{oo},x_{oi},R_A,0) - V(x_{io},x_{ii},r_A,0) - V(x_{ii},x_{oi},r_B,R)$$

Case V $(r_A < R - r_B < R_A)$

$$V^{V} = V(x_{io},x_{oo},R_B,R) + V(x_{oo},x_{oi},R_A,0) - V(x_{io},r_A,r_A,0) - V(R - r_B,x_{oi},r_B,R)$$

Case VI $(r_A \le R - R_B < R_A)$

$$V^{VI} = V(R - R_B,x_{oo},R_B,R) + V(x_{oo},R_A,R_A,0)$$

Case VII $(R_A \le R - R_B)$

$$V^{VII} = 0$$

In practice, 2D pair distributions are averaged over an entire molecular dynamics trajectory, for which reason the 2D pair distribution histogram will have to be normalized with the number of trajectory frames included and by the water density in the simulation.

Results and Discussion

Dynamics of the α-(1-1)-α Glycosidic Linkage. *Adiabatic Map*. Figure 3A displays the adiabatic map of trehalose in a vacuum in the applied force field. It has a characteristic symmetric "skull" shape and is consistent with the previously published adiabatic map[24] using the same force field but a different definition of the Φ and Φ′. The map has three significant potential energy wells. (1) This is the almost ellipsoid "brain" including the symmetric global energy minimum (***V***) at (Φ, Φ′) = (180, 180); this structure is shown in Figure 1A. (2) This is the "eye" wells having local minima at (Φ, Φ′) = (100, 160) and (Φ, Φ′) = (160, 100) being only 3.65 kcal/mol above the global minimum. (3) This is the "mouth" well which accommodates the locations of the known crystal structures (the trehalose dihydrate marked with a ***D*** and the trehalose anhydrate marked with an ***A***) and has a local minimum at (Φ, Φ′) = (100, 160), 3.19 kcal/mol above the global minimum. The adiabatic map has been scrutinized by Liu et al.[24] We will only mention here that the global minimum in a vacuum is not the one found

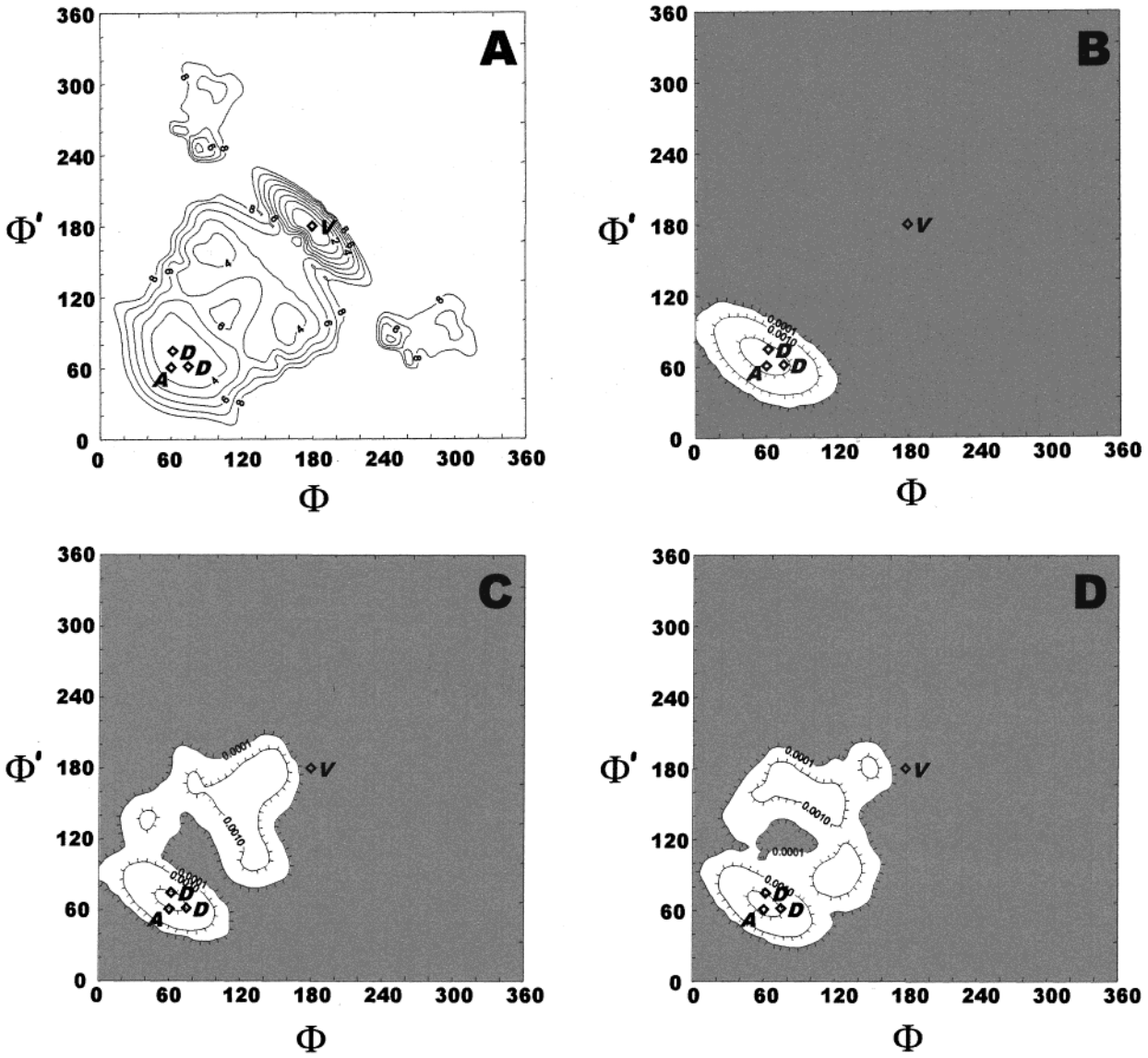

Figure 3. (A) Adiabatic map of α,α-trehalose in a vacuum as a function of Φ and Φ′. (B). Population density maps of α,α-trehalose SX trajectory in aqueous solution as a function of Φ and Φ′. Contours are drawn in 1 kcal/mol intervals. (C) Population density maps of α,α-trehalose S1 trajectory in aqueous solution as a function of Φ and Φ′. (D) Population density maps of α,α-trehalose S2 trajectory in aqueous solution as a function of Φ and Φ′. All figures include positions of the anhydrous (***A***) and dihydrate (***D***) crystal structures as well as the global minimum from the adiabatic grid search (***V***).

in other force fields: (Φ, Φ′) = (61, 61)[18] and (Φ, Φ′) = (76, 76)[19] or the observed experimental conformation from X-ray: (Φ, Φ′) = (60, 61),[10] or estimated from optical rotation: (Φ, Φ′) = (60, 60)[16] and from NMR (Φ, Φ′) = (79, 79).[17] All of these are (approximately) symmetric and located in the secondary "mouth" well.

Population Maps. Figure 3B displays the population density map of the 1 ns trajectory starting from the crystal conformation of the dihydrate. From the figure we observe that the presence of water is modifying the mean potential acting on the trehalose solute and the population contours have become almost ellipsoid in contrast to the "mouth-shaped" well on the adiabatic map in Figure 3A. The trajectory does not undergo any excursions from the "mouth" well and, as apparent from the figure, we observed a slight but significant asymmetry in the dihedral conformation of the trehalose solute induced by the presence of water. The maximum population is located off-diagonal at (Φ, Φ′) = (60, 70) close to the location of the dihydrate structure. The average trajectory geometry of the dihedral linkage is listed in Table 1 and also indicates a weakly but unambiguous asymmetric mean structure (Φ, Φ′) = (56, 65). This is a very significant result that evidences the generation of an asymmetric mean structure from the interaction between the two symmetric molecules, water and trehalose, as is also found in the dihydrate crystal structure. The correlation in the movements across the dihedral linkage (between the time series of Φ and Φ′) is calculated to $r = -0.67$ which is a relatively high negative correlation (when

TABLE 1: Trehalose Conformations (distances are in angstrøms and angles are in degrees)

conformation	dihydrate crystal[8]	anhydrous crystal[10]	minimum in a vacuum	average MD[a]
Φ	61.7	60.1	180	56 (17)
Φ′	74.8	60.8	180	65 (12)
E(Φ,Φ′)[b]	3.2	3.4	0.0	∼3.6
θ	115.8	113.3	118.9	115.3 (3.0)
ω_g	69.8	71.0	179.4	−101 (56)
$\omega_{g'}$	−75.6	−72.1	171.4	−134 (69)

[a] RMS fluctuations are given in parentheses. [b] Potential energy on the adiabatic map considering only the glycosidic conformation (Φ, Φ′).

TABLE 2: Measured and Calculated 3*J* Coupling Constants (Hz) of α,α-Trehalose

	MS in a vacuum		MS in water		experimental	
^3J-couplings	Glc*p*	Glc*p*′	Glc*p*	Glc*p*′	ref 15	ref 46
H-1,H-2	2.9	2.9	3.2	3.2	3.6	3.6
H-2,H-3	10.5	10.5	10.0	10.0	9.3	9.7
H-3,H-4	9.8	9.8	9.5	9.5	9.3	9.6
H-4,H-5	9.8	9.8	9.6	9.7	9.3	9.6
H-5,H-6R	4.3	4.3	2.6	3.1	4.5	
H-5,H-6S	10.7	10.7	5.2	6.3	2.2	
GG:GT:TG[a]	7:−7:100	7:−7:100	65:5:30	52:4:44	68:41:−9	
GG:GT:TG	3:0:97	3:0:97	70:0:30	52:2:46		
C-1,H-1′	1.5	1.5	2.2	2.3	2.5[b]	3.3[c]
C-5,H-1	6.8	6.8	6.7	6.7	7.0[d†]	

[a] Population ratio back-calculated from pro-R and pro-S couplings. [B] From Parfondry et al.[38] [c] From Batta et al.[17] Estimated uncertainty was given as ±0.5 Hz. [d] From Mulloy et al.[47]

Φ increases, Φ′ decreases, and vice versa), especially when compared to the totally uncorrelated ($r = -0.05$) situation in a similar simulation of sucrose. This result indicates a high degree of cooperative movements between the two pyranose rings. In addition, it is noteworthy (Table I) that the C-1g−O-1g−C-1g′ angle which was calculated to 118.9° in the global energy minimum with the explicit presence of water is reduced to a mean value of 115.3°, in good agreement with the angle in the dihydrate structure. Two 0.75 ns trajectories started in the global in a vacuum minimum (Figure 1A) both reverted to the "mouth" well where they stayed for the remaining simulation time (Figure 3C,D).

Heteronuclear Coupling Constants. From the adiabatic map (Figure 3A) and the 1 ns simulation (Figure 3B) we calculated ^3J coupling constants using a Karplus type of equation. The heteronuclear coupling over the dihedral linkage (C−O−C−H) which was calculated to 1.5 Hz from the vacuum simulation increased to 2.2/2.3 Hz in the MD simulation which has to be compared with the experimental value of 2.5 Hz measured by Parfondry et al.[38] and the more recent determination of 3.3 Hz by Batta et al.,[17] a somewhat poorer calculation than for sucrose. The intra-ring C-5−H-1 heteronuclear coupling[44] was calculated with good precision and was, as expected ($^4C_1$), not affected by the presence of the water solvent.

Solute Dynamics. *Homonuclear Coupling Constants*. From the adiabatic map (Figure 3A) and the 1 ns simulation (Figure 3B) the ^3J coupling constants were calculated using a Karplus type of equation (Table 2). For the pyranosyl H−C−C−H couplings we observe a fair agreement with both the vacuum simulation and the MD simulation consistent with the preservation of the $^4C_1$ chair conformation. For the primary hydroxyl couplings we observe, as in the case of sucrose, that the two couplings have switched around due to a relatively large population of TG conformers. By comparison with the vacuum data we notice that the presence of water promotes GG conformations which is close to the expected experimental finding of approximately 60%, but the expected population of approximately 40% GT conformations is switched to TG conformers. An identical pattern was previously observed in the sucrose simulation.[35]

Diffusion. The translational diffusion of trehalose in water has recently been accessed experimentally to approximately 3×10^{-6} cm^2/s by Megazu et al.[39] for a 0.02 volume fraction and to approximately 4×10^{-6} cm^2/s by Rampp et al. [40] for a 10% (w/w) solution. The calculated translational diffusion of trehalose from the molecular dynamics simulation (Figure 4A) of approximately $(5.0-5.2) \times 10^{-6}$ cm^2/s is very similar to that of sucrose which is in good agreement with the fact that at low concentrations the translational diffusion of the four nonreducing disaccharides—sucrose, allosucrose, leucrose, and α,α-trehalose—are quite similar.[40] In contrast, the rotational diffusion (Figure 4B) appears to be much slower than for sucrose. The latter feature appears to be in good accordance with the experimental differences where the overall correlation time, as derived from NMR experiments by Batta et al.,[17] was estimated in the range of 400−500 ps.

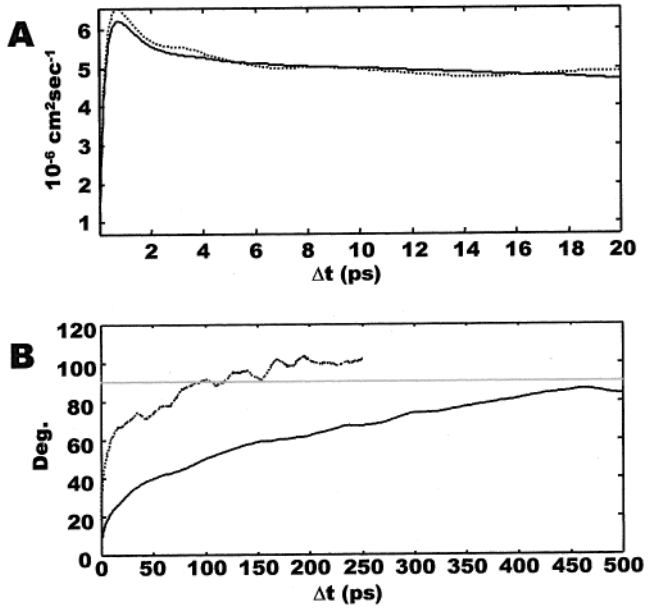

Figure 4. Trehalose diffusion: (A) Calculated translational diffusion of trehalose compared to that of sucrose (dotted line), and (B) calculated rotational diffusion of the dipole moment vector compared to that of sucrose (dotted line).

Trehalose Hydration Characteristics. The calculated radial pair distributions of acetalic and hydroxylic trehalose oxygen atoms with respect to water oxygen atoms (Figure 5) appear typical in shape. The pair distributions of the hydroxylic oxygen atoms display typical hydrophilic interaction with a well-defined first hydration shell with a density peak at 2.8 Å and a density minimum at approximately 3.5 Å. At this distance, the water density has decreased to a little more than half of the bulk water density. The water distribution around the three acetalic oxygen atoms are perturbed due to steric effects and donating only characteristics and especially the glycosidic oxygen, O-1g, is particularly perturbed. From the radial point of view the two acetalic ring oxygen atoms appear to be normally hydrated; however, in the calculated orientational distribution functions, Figure 6, the water molecules around the two acetalic ring oxygen display an unusual lack of structure. In molecules that we have investigated so far, including sucrose, we observe more

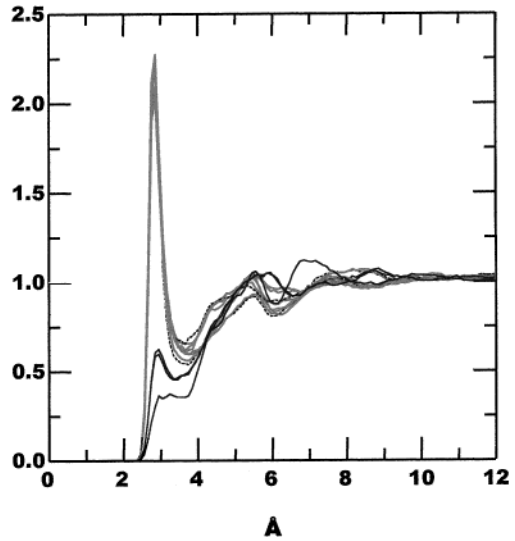

Figure 5. Radial pair distribution functions *g(r)* of water-oxygen atoms around solute oxygen atoms. Distances (*x*-axis) are in angstrøms.

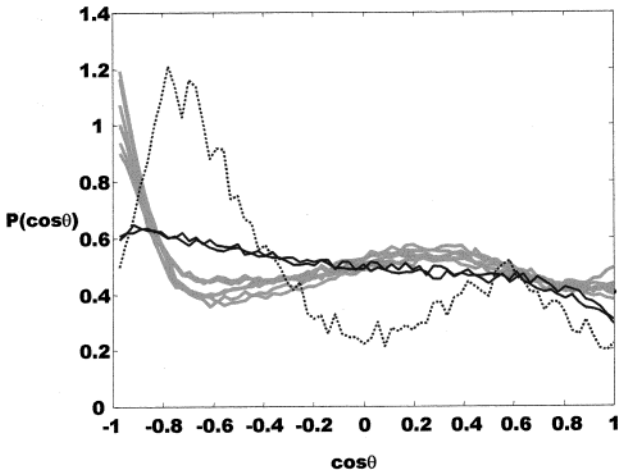

Figure 6. Orientational O_w-H...O distribution functions $p(\cos\theta)$ of water molecules in the first hydration shell (defined by radii of 3.5 Å) around solute oxygen atoms. Distribution around O-1g (black dotted line), O-5g (black), and hydroxyl oxygen atoms (gray).

structure (similar to the orientational distribution around O-1g) around the ring oxygen atoms.

We then calculated the global average hydration number for the trehalose simulation, taking into account water oxygen atoms around all 8 solute oxygen atoms. Figure 7A shows the hydration number of trehalose as a function of distance from solute oxygen atoms, and Figure 7B shows the first derivatives. The latter curve which is sensitive to changes in the buildup of water density reveals two peaks corresponding to the first and second hydration shells. For comparison, the results from the sucrose simulation (dotted line) are superimposed on the trehalose results. As apparent from the figures only a very minor difference in global mean hydration was calculated, indicating that this number is mainly affected by the number of different solute oxygen atoms and is not able to monitor the differences in experimentally derived hydration numbers between sucrose and trehalose. A plethora of literature reports exists on the hydration number for sucrose,[41] and two studies include both the hydration number for sucrose ($h = 6.8$;[28] $h = 6.33$)[42] and trehalose ($h = 8.0$;[28] $h = 7.95$),[42] respectively. Most recently the hydration number of trehalose has been determined to 12.5 by Megazú et al.[43] from ultrasonic measurements. Using the minimum ($R < 3.5$ Å) and maximum ($R < 2.8$ Å) of the first hydration shell as defined by the radial pair distributions, we obtained almost exactly the same numbers as in the sucrose simulation, 27.5 and 7.8, respectively.

TABLE 3: Average (t_{av}) and Maximum (t_{max}) Residence Times for Water Molecules in the First Hydration Shell around Solute Oxygens ($R < 3.5$ Å)[a]

	sucrose		trehalose	
atom	t_{max}	t_{av}	t_{max}	t_{av}
O-1g	9.36	0.41	17.26	0.32
O-2g/g′	15.00	0.68	27.20/23.02	0.69/0.69
O-3g/g′	18.16	0.63	19.28/16.60	0.64/0.66
O-4g/g′	18.14	0.64	17.54/16.82	0.61/0.62
O-5g/g′	13.30	0.46	10.18/8.02	0.37/0.36
O-6g/g′	17.20	0.60	18.54/22.40	0.61/0.61
O_w...O_w	24.82	0.54	29.38	0.55

[a] Times are in picoseconds.

Residence Times for Water Molecules around the Trehalose Solute. To assess the dynamic aspect of the first hydration shell we calculated the maximal and average residence times for all water molecules in the first hydration shell ($R < 3.5$ Å). The results listed in Table 3 reveal differences in the average residence times ranging from 0.32 ps around O-1g to 0.69 ps around O-2g/O-2g′. The estimated standard deviations for the residence times is estimated to approximately 0.002 ps. By comparison with sucrose, the residence times for water molecules around O-2g are slightly increased at the expense of the

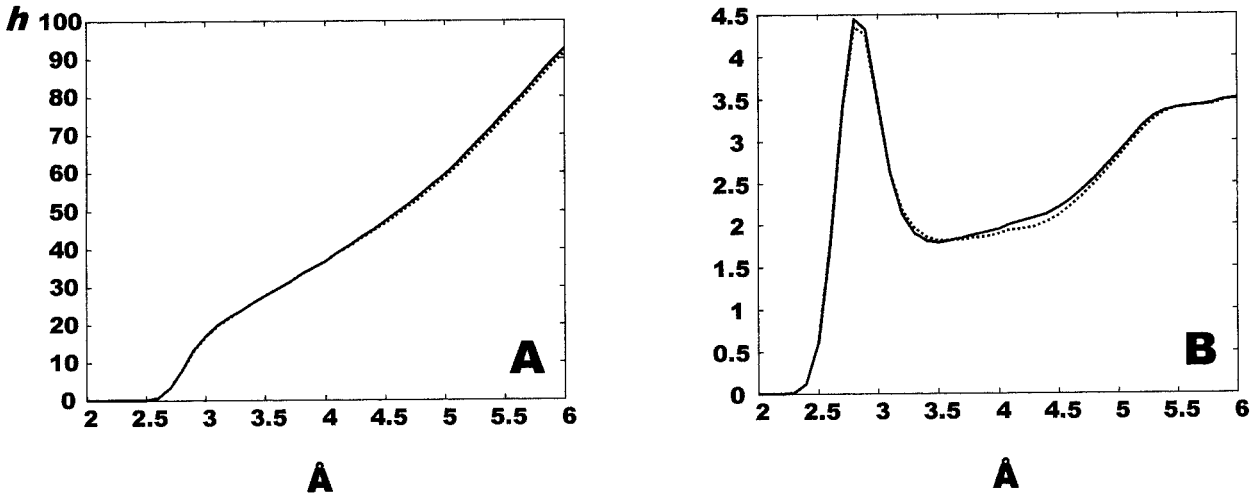

Figure 7. (A) The average number of water molecules as a function of the distance from the solute oxygen atoms. (B) The first derivative of (A). Sucrose data are indicated with a dotted line.

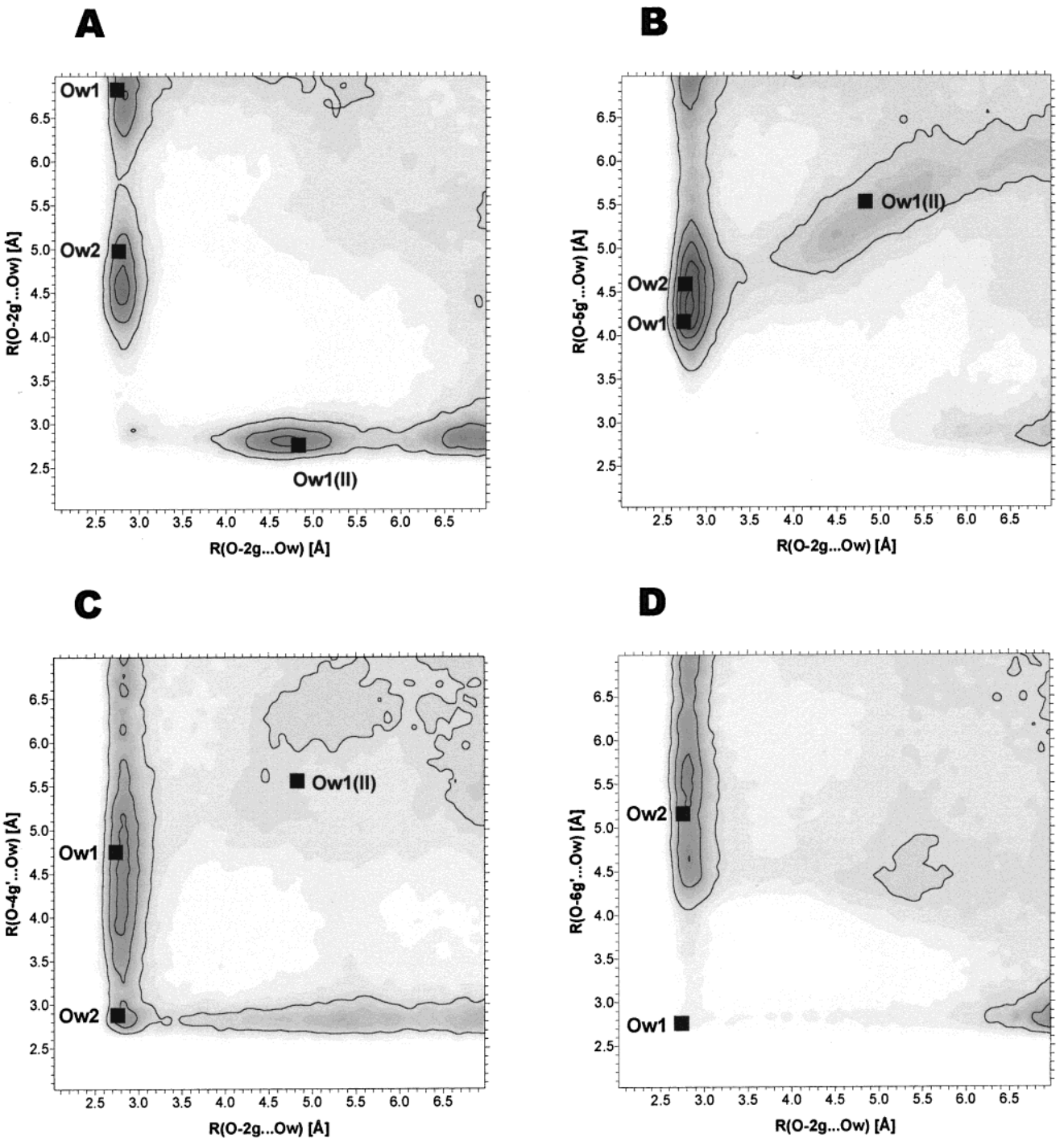

Figure 8. Normalized 2D pair distributions: (A) the O-2g...O_w...O-2g′ distribution, (B) the O-2g...O_w...O-5g′ distribution, (C) the O-2g...O_w...O-g′ distribution, and (D) the O-2g...O_w...O-6g′ distribution. Distances are in angstrøms.

average residence time for waters around O-4g and to the benefit of the residence time around O-3g. The variations in the maximum residence times reflect the same trend albeit stronger. The residence times for waters around the relatively free primary hydroxyl oxygen are longer for trehalose—0.610(2) ps for O-6g and 0.609(2) ps for O-6g′. By comparison with sucrose, the water residence characteristics around the primary hydroxyl groups are found to be slightly longer (0.611(2) ps and 0.610-(2) ps, respectively), which is also reflected in the maximum residence times. Interestingly this is also the case for water—water interactions that exhibit slightly longer residence characteristics in the trehalose trajectory: 0.552(2) ps as compared to 0.544(2) ps for the sucrose trajectory and might reflect a minor change in the long-range order of the water. Using this number as a reference we observe that average residence times for water molecules around trehalose hydroxyl groups are increased with up to 25% (O-2g) and decreased with up to 42% around the acetalic oxygens (O-1g). From Table 3 it is evident that the very long residence characteristics around O-2g/g′ is a significant feature to trehalose hydration. It has the only symmetric residence characteristic and it might be argued that they act as anchor points (O-2g and O-2g′) in the pseudo tetrahedral water lattice which in turn could explain the apparent anisotropy of the molecular tumbling (vide infra). However, the most notable difference between the sucrose and trehalose residence characteristics is the very short residence times around the acetalic oxygens. Again, this could be explained by a relatively high flux of passing water molecules "circulating"

TABLE 4: Crystalline Trehalose-Oxygen Water-Oxygen Distances in the Hydrated Environment of Trehalose in the Dihydrate Crystal Structure[8,a]

conformation	accepting/ donating	symmetry operation[b]	distance
O-2g...O_w1	D	**II**	2.76
O-2g...O_w1	A	**I**+**c**	2.70
O-2g′...O_w1	A	**I**	2.76
O-2g′...O_w2	D	**I**	2.74
O-3g′...O_w2	A	**IV**	2.80
O-4g...O_w1	D	**I**	2.88
O-6g...O_w2	A	**I**	2.76

[a] The space group is $P2_12_12_1$, with four trehalose and 8 water molecules in a unit cell having dimensions of $a = 12.230$ (2), $b = 17.890$ (3), and $c = 7.596$ (1) Å. Distances are in angstrøms. [b] Symmetry operations: **I**: (x,y,z); **II**: $(-x + 1/2, -y, z + 1/2)$; **III**: $(-x, y + 1/2, -z + 1/2)$; **IV**: $(x + 1/2, -y + 1/2, -z)$.

around the central cavity (O-5g...O-1g...O-5g′) between the two pyranose rings while trehalose exhibit rotational diffusion around the O-2g...O-2g′ axis (see Figure 1).

2D Radial Pair Distributions. We then calculated 2D pair distributions[29] with all different combinations of solute oxygen pairs, looking for strong shared or localized water density sites. Only minor differences were observed due to the asymmetric hydration, and Figure 8 summarizes the main hydration features of trehalose. Fig. 8A shows the normalized 2D radial pair distribution of water in which the solute atoms O-2 g and O-2 g′ are the reference sites. In the trajectory the average O-2 g...O-2 g′ distance was 5.47 Å, ranging from 4.27 to 6.31 Å, indicating that a geometrical situation with a bridging water is possible. From the highly symmetric contour plot it is revealed that a shared water density in the first hydration shell (water bridge) is possible, but that the magnitude of such a shared water density only adds up to approximately the bulk water density (1.0); therefore, this is not a significant feature. The fact that the peak is moved upward to (2.9 Å, 2.9 Å) suggests that such a situation is sterically and entropically restricted to be a dominating hydration feature. Maximum water densities of 3.6 and 3.2 are found at the locations (2.8 Å, 4.6 Å) and (4.7 Å, 2.8 Å), respectively, including a second long range structure of approximately 3 in the vicinity of (2.8 Å, 6.8 Å). All these maximum water density regions represent hydration sites present in the trehalose dihydrate crystal which, in the plot, are indicated by the water molecules O_w1, O_w2 and O_w1(II) (Figure 1B and Table 4). In the crystal structure these three water molecules are almost perfectly axially positioned above the O-2g, O-4g, and O-6g groups of one glucopyranosyl group and bridging (mainly) to the O-2g′ group of the second perpendicular glucopyranosyl residue.

Another significant 2D pair distribution is displayed in Figure 8B describing water densities with respect to the solute oxygen atoms O-2g and O-5g′. It mainly consists of two features: a localized water density region with a maximum density of 5.1 at (2.8 Å; 4.2 Å) which was the highest inter-residue density found in this MD simulation and a diagonal long-range water density contour surmounting up to 1.6 times the bulk water density as far as (5.5 Å; 5.7 Å). The first density region encompasses both O_w1 and O_w2 hydration sites from the dihydrate structure and can be considered as a band of favorable first hydration shell interactions between water molecules around O-2g and O-4g′ and O-6g′ consistent with the water density contours previously described by Liu et al.[23] In the trajectory, the average O-2g...O-5g′ distance was 4.42 Å, ranging from 3.28 to 5.37 Å indicating that a first hydration shell interaction is possible. In this case, however, the first hydration shell bridging is absent, indicating that water density is removed from O-5g into the hydration band represented by the water molecules O_w1, O_w2 and O_w1(II). This finding is corroborated by the unusually flat orientational distribution of water around the ring oxygen atoms (Figure 6). The significant long-range diagonal water density where the O_w1(II) is found indicates that the O-2g...O-5g′ vector is a highly conserved structural motif with respect to the water structure.

In the 2D pair distribution plot in Fig. 8C calculated with respect to O-2 g and O-4 g′ we find the most significant shared water molecule which corresponds to the location of the water molecule Ow2 in the crystal structure of the dihydrate form of trehalose. The maximum density of the shared water is calculated to 2.4 which is quite low compared to the shared water density of sucrose of 8.5;[29] this is probably not a single determinant factor in the stabilization of the trehalose solution conformation. The magnitude of this shared density is only slightly stronger than the 1D pair distribution peak density of approximately 2.2 of the first hydration shell (Figure 5). The elongated feature at (2.8 Å, 3.3 → 5.8 Å) with a maximum density of 3.7 encompass the O_w1 water and indicates a large flexibility of the hydration site between O-2g and O-6g′. The average O-2g...O-4g′ distance was calculated to 5.51 Å, ranging from 3.69 to 7.26 Å and indicates a rather flexible situation going from the "locked" bridging situation to a more open structure.

Figure 8D displays the 2D pair distributions with respect to O-2g and O-6g′ which in fact was the only map 2D radial distribution map displaying substantial asymmetry when compared to the symmetric counterpart: the O-2g′...O-6g map. Although the primary hydroxyl groups are the most flexible points in the trehalose structure this symmetry just underlines that our trajectory unfortunately was not carried far enough to pass the symmetrical barrier of water plus trehalose. For example, the maximum first hydration shell shared density is approximately 1.8, whereas it only adds up to 0.6 in the O-2g′...O_w...O-6g map. In the crystal structure of the dihydrate, this bridging position is occupied by O_w1 to satisfy the hydration need of the solute. However, the magnitude of this hydration site indicates that it is probably not a single determinant factor in the stabilization of the trehalose solution conformation. The elongated feature at (2.8 Å, 4.3 Å → 6.5 Å) with a maximum density of 2.5 again indicates a rather flexible hydration site along O-6g′. In the trajectory the average O-2g...O-6g′ distance was 5.92 Å, ranging from a direct hydrogen bond of 2.83 Å up to 8.08 Å with no hydration shell interactions.

It can be stressed that the structuring imposed on the water by trehalose (or vice versa) is quite complex and that no strong first hydration shell interactions dominate the solution structure of trehalose. This corroborates previous findings by Liu et al.[24] who investigated the hydration pattern of trehalose using a solvent density mapping different from ours. The average hydration characteristics of trehalose is rather to be considered as a concerted action including especially the hydration sites which in the solid state is occupied by O_w1, O_w2, and O_w1(II). The most significant result of this analysis is the fact that the trehalose hydration pattern in dilute solution is surprisingly close to that of the solid-state dihydrate structure.

Conclusions

It has been the aim of the present work to establish through molecular modeling the structural and dynamical features of trehalose in dilute aqueous solution. From a 2.5 ns simulation with explicit water molecules, it has been shown that the low-energy region of the (Φ, Φ')-space is weakly but significantly

asymmetric with respect to the calculation performed in a vacuum. Quite interestingly, such an asymmetry is also observed in the crystalline conformation of a dihydrate allomorph of trehalose. The trehalose molecule is extensively bound to water molecules. On average, around 25 water molecules constitute the first hydration shell. Clearly, all the potential intramolecular hydrogen bonds are exchanged to these surrounding water molecules. The hydroxyl groups of the disaccharide are extensively hydrogen bonded to solvent in all the stable equilibrium conformations. The residence times of hydrogen binding between water molecules and oxygen atoms from the solute do not show any major variations except those around the O-2g which are about two times longer than normal. Part of this behavior could be explained by the use of 2D radial pair distributions that have been devised to examine the hydration behavior in the condensed-phase molecular dynamics simulation. Some strong anisotropic solvent density was detected for all those water molecules that can make bridging hydrogen bonds between secondary hydroxyl groups on different monosaccharides. This could provide a molecular explanation to the anisotropy of tumbling of trehalose. In terms of hydration, there exists a very close similarity of the crystal dihydrate structure of trehalose to that in the diluted solution in the MD simulations, indicating that trehalose is almost perfectly hydrated in the dihydrate crystal.

Extensive comparison with the hydration patterns of another nonreducing disaccharide, sucrose, failed to highlight any striking structural features that could explain the cryoprotective and antidesiccations properties of trehalose. However, these calculations strongly suggest (a) that trehalose has a significant longer (and anisotropic) rotational diffusion time, (b) that trehalose conformation in dilute solution is not dominated by a specific inter-ring (first hydration shell) water interaction, and (c) perhaps most important that trehalose appears to be near perfect hydrated in the dihydrate solid state. The particular hydration compatibility between the solution state and the solid state of trehalose suggest that trehalose at ambient temperatures can change state (at 2 H_2O per trehalose) with practically no consequences for trehalose but where two water molecules are trapped. The latter observation may explain the trehalose glass-transition anomaly[5] and the large potential of trehalose to retain internal waters,[44] both mechanisms play a key role in the ability of trehalose to protect biological life/activity against dehydration and freezing. In light of these findings, at present the most favored theory about trehalose activity, namely, the "water replacement theory",[45] should rather be the "trehalose water-trap theory" as trehalose, unlike other sugars, is extraordinarily reluctant to lose the last two waters. Moreover, the position of these two waters need not to be highly localized to satisfy the hydration "needs" of trehalose, thus preserving some water activity. An obvious extension to this work would therefore be to simulate the α,α-trehalose·$2H_2O$ glass.

Acknowledgment. S.B.E. was supported by the Centre of Advanced Food Studies (LMC) in a project concerning molecular modeling of carbohydrates. S.P. acknowledges the support of CNRS through the Program " Physique et Chimie du Vivant".

References and Notes

(1) Crowe, J. H.; Crowe, L. M.; Chapman, D. Preservation of membranes in anhydrobiotic organisms: the role of trehalose. *Science* **1984**, *223*, 701−703.

(2) Crowe, L. M.; Mouradian, R.; Crowe, J. H.; Jackson, S. A.; Womersley, C. Effects of carbohydrates on membrane stability at low water activity. *Biochim. Biophys. Acta* **1984**, *947*, 367−384.

(3) Crowe, J. H.; Crowe, L. M.; Carpenter, J. F. Stabilization of dry phospholipid bilayers and proteins by sugars. *Biochem. J.* **1987**, *242*, 1−10.

(4) Nakagaki, M.; Nagase, H.; Ueda, H. Stabilization of the lamellar structure of phosphatidylcholine by complex-formation with trehalose. *J. Membr. Sci.* **1992**, *73* (2−3), 173−180.

(5) Green, J. L.; Angell, C. A. Phase Relations and Vitrification in Saccharide-Water Solutions and the Trehalose Anormaly. *J. Phys. Chem.* **1989**, *93*, 2880−2882.

(6) Roser, B. Trehalose, a new approach to premium dried foods. *Trends Food Sci. Technol.* **1991**, *2*, 66−69.

(7) Crowe, J. H.; Crowe, L. M. Preservation of mammalian cells − learning nature's tricks. *Nature Biotech.* **2000**, *18* (2), 145−146.

(8) Brown, G. M.; Rohrer, D. C.; Berking, B.; Beevers, C. A.; Gould, R. O.; Simpson, R. The Crystal Structure of α,α-Trehalose Dihydrate from Three Independent X-ray Determinations. *Acta Crystallogr., Sect. B.* **1972**, *28*, 3145−3158.

(9) Taga, T.; Senma, M.; Osaki, K. The crystal and molecular structure of trehalose dihydrate. *Acta Crystallogr., Sect. B.* **1972**, *28*, 3258−3263.

(10) Jeffrey, G. A.; Nanni, R. The Crystal Structure of Anhydrous α,α-Trehalose at −150°. *Carbohydr. Res.* **1985**, *137*, 21−30.

(11) Crowe, J. H.; Crowe, L. M.; Chapman, D. Infrared spectroscopic studies on the interaction of water and carbohydrates with a biological membrane. *Arch. Biochem. Biophys.* **1984**, *232*, 400−407.

(12) Belton, P. S.; Gil, A. M. IR and Raman Spectroscopic Studies of the Interaction of Trehalose with Hen Egg White Lysozyme. *Biopolymers* **1994**, *34*, 957−961.

(13) Lee, C. W. B.; Waugh, J. S.; Griffin, R. G. Solid-state NMR study of trehalose/1,2-dipalmitoyl-*sn*-phosphatidylcholine interactions. *Biochemistry* **1986**, *25*, 3737−3742.

(14) Lee, C. W. B.; Dus Gupta, S. K.; Mattai, J.; Shipley, G. G.; Abdel-Mageed, O. H.; Makriyannis, A.; Griffin, R. G. Characterization of the L_λ phase in trehalose-stabilized dry membranes by solid-state NMR and X-ray diffraction. *Biochemistry* **1989**, *28*, 5000−5009.

(15) Bock, K.; Defaye, J.; Driquez, H.; Bar-Guilloux, E. Conformations in Solution of α,α-Trehalose, α-D-Glucopyranosyl α-D-Mannopyranoside, and Their 1-Thioglycosyl Analogues, and a Tentative Correlation of Their Behavior with Respect to the Enzyme Trehalase. *Eur. J. Biochem.* **1983**, *131*, 595−600.

(16) Duda, C. A.; Stevens, E. S. Trehalose Conformation in Aqueous Solution from Optical Rotation. *J. Am. Chem. Soc.* **1990**, *112*, 7406−7407.

(17) Batta, G. J.; Kövér, K. E.; Gervay, J.; Hornyák, M.; Roberts, G. M. Temperature Dependence of Molecular Conformation, Dynamics, and Chemical Shift Anisotropy of α,α-Trehalose in D_2O by NMR Relaxation. *J. Am. Chem. Soc.* **1997**, *119*, 1336−1345.

(18) Tvaroska, I.; Vaclavik, L. Stereochemistry of Nonreducing Disaccharides in Solution. *Carbohydr. Res.* **1987**, *160*, 137−149.

(19) Dowd, M. K.; Reilly, P. J.; French, A. D. Conformational Analysis of Trehalose Disaccharides and Analogues Using MM3. *J. Comput. Chem.* **1992**, *13* (1), 102−114.

(20) Rudolph, B. R.; Chandrasekhar, J.; Gaber, B. P.; Nagumo, M. Molecular modelling of saccharide-lipid interactions. *Chem. Phys. Lipids* **1990**, *53* (2−3), 243−261.

(21) Donnamaria, M. C.; Howard, E. I.; Grigera, J. R. Interaction of Water with α,α-Trehalose in Solution: Molecular Dynamics Approach. *J. Chem. Soc. Faraday Trans.* **1994**, *90* (18), 2731−2735.

(22) van Gunsteren, W. F.; Berendsen, H. J. C. Groningen Molecular Simulation (GROMOS) Program Package. 1987.

(23) Berendsen, H. J. C.; Grigera, J. R.; Straatsma, T. P. The missing term in effective pair potentials. *J. Phys. Chem.* **1987**, *91*, 6269−6271.

(24) Liu, Q.; Schmidt, R. K.; Teo, B.; Karplus, P. A.; Brady, J. W. Molecular Dynamics Studies of the Hydration of α,α-Trehalose. *J. Am. Chem. Soc.* **1997**, *119*, 7851−7862.

(25) Ha, S. N.; Giammona, A.; Field, M.; Brady, J. W. A revised potential-energy surface for molecular mechanics of carbohydrates. *Carbohydr. Res.* **1988**, *180* (2), 207−221.

(26) Jorgensen, W. L.; Chandrasekhar, J.; Madura, J. D.; Impey, R. W.; Klein, M. L. Comparison of simple potential functions for simulating liquid water. *J. Chem. Phys.* **1983**, *79* (2), 926−935.

(27) Engelsen, S. B.; Pérez, S. The Hydration of Sucrose. *Carbohydr. Res.* **1996**, *292*, 21−38.

(28) Portmann, M.-O.; Birch, G. Sweet Taste and Solution Properties of α,α-Trehalose. *J. Sci. Food Agric.* **1995**, *69*, 275−281.

(29) Andersson, C. A.; Engelsen, S. B. The mean hydration of carbohydrates as studied by normalized two-dimensional radial pair distributions. *J. Mol. Graph. Model.* **1999**, *17*, 101−105.

(30) IUPAC−IUB Nomenclature of Carbohydrates. *Carbohydr. Res.* **1997**, *297*, 1−92.

(31) Brooks, B. R.; Bruccoleri, R. E.; Olafson, B. D.; States, D. J.; Swaminathan, S.; Karplus, M. CHARMM: A Program for Macromolecular Energy, Minimization and Dynamics Calculations. *J. Comput. Chem.* **1983**, *4* (2), 187−217.

(32) Verlet, L. Computer Experiments on Classical Fluids. I. Thermodynamical Properties of Lennard-Jones Molecules. *Phys. Rev.* **1967**, *159* (1), 98−103.

(33) van Gunsteren, W. F.; Berendsen, H. J. C. Algorithms for macromolecular dynamics and constraint dynamics. *Mol. Phys.* **1977**, *34* (5), 1311−1327.

(34) Allen, M. P.; Tildesley, D. J. *Computer Simulations of Liquids*; Clarenden Press: Oxford, U.K., 1987.

(35) Engelsen, S. B.; Hervé du Penhoat, C.; Pérez, S. Molecular Relaxation of Sucrose in Aqueous Solution: How a Nanosecond Molecular Dynamics Simulation Helps To Reconcile NMR Data. *J. Phys. Chem.* **1995**, *99*, 13334−13351.

(36) Haasnoot, C. A. G.; de Leeuw, F. A. A. M.; Altona, C. The relationship between proton−proton NMR coupling constants and substituent electronegativities. An empirical generalization of the Karplus equation. *Tetrahedron* **1980**, *36*, 2783−2792.

(37) Tvaroska, I.; Hricovini, M.; Petrakova, E. An attempt to derive a new Karplus-type equation of vicinal proton-carbon coupling constants for C−O−C−H segments of bonded atoms. *Carbohydr. Res.* **1989**, *189*, 359−362.

(38) Parfondry, A.; Cyr, N.; Perlin, A. S. ^{13}C-^{1}H Interresidue Coupling in Disaccharides, and the Orientations of Glycosidic Bonds. *Carbohydr. Res.* **1977**, *59*, 299−309.

(39) Magazù, S.; Maisano, G.; Middendorf, H. D.; Migliardo, P.; Musolino, A. M.; Villari, V. α,α-Trehalose-Water Solutions. II. Influence of Hydrogen Bond Connectivity on Transport Properties. *J. Phys. Chem.* **1998**, *102*, 2060−2063.

(40) Rampp, M.; Buttersack, C.; Lüdemann, H.-D. c,T.-Dependence of the Viscosity and the Self-Diffusion Coefficients in Some Aqueous Carbohydrate Solutions. *Carbohydr. Res.* **2000**, in press.

(41) Engelsen, S. B.; Pérez, S. Internal motions and hydration of sucrose in a diluted water solution. *J. Mol. Graph. Model.* **1997**, *15*, 122−131.

(42) Kawai, H.; Sakurai, M.; Inoue, Y.; Chûjô, R.; Kobayashi, S. Hydration of Oligosaccharides: Anormalous Hydration Ability of Trehalose. *Cryobiology* **1992**, *29*, 599−606.

(43) Magazù, S.; Migliardo, P.; Musolino, A. M.; Sciortino, M. T. α,α-Trehalose-Water Solutions. 1. Hydration Phenomena and Anomalies in the Acoustic Properties. *J. Phys. Chem.* **1997**, *101*, 2348−2351.

(44) Sastry, G. M.; Agmon, N. Trehalose Prevents Myoglobin Collapse and Preserves Its Internal Mobility. *Biochemistry* **1997**, *36*, 7097−7108.

(45) Tsvetkova, N. M.; Phillips, B. L.; Crowe, L. M.; Crowe, J. H.; Risbud, S. H. Effect of sugars on headgroup mobility in freeze-dried dipalmitoylphosphatidylcholine bilayers: Solid-state P-31 NMR and FTIR studies. *Biophys. J.* **1998**, *75* (6), 2947−2955.

(46) Tarelli, E.; Wheeler, S. F. The preparation of the four monophosphates of α,α′-trehalose from trehalose and sodium phosphate. *Carbohydr. Res.* **1994**, *261*, 25−36.

(47) Mulloy, B.; Frenkiel, T. A.; Davies, D. B. Long-Range Carbon-Proton Coupling Constants: Application to Conformational Studies of Oligosaccharides. *Carbohydr. Res.* **1988**, *184*, 39−46.